Design of Microstructured Flat Optical Fiber for Multiaxial Strain Monitoring in Composite Materials

Francesco Anelli , Andrea Annunziato , Alessia Erario, Christopher Holmes , Caterina Ciminelli , and Francesco Prudenzano , *Member, IEEE*

Abstract—An innovative microstructured flat optical fiber is designed to obtain a multiaxial strain sensor for composite material monitoring. The sensing regions are constituted by the two eyelets where Bragg gratings are written. To achieve multiaxial sensing, a suitable microstructure is designed close to only one of the eyelets. The effect of the strain field, evaluated via a 3D finite element method approach, is considered to obtain the change of the refractive index distribution. The electromagnetic modal analysis and the coupled mode theory are exploited to evaluate the Bragg wavelength shift for the slow and fast axis fundamental modes, guided in the two eyelets and affecting the sensor response. The designed microstructured flat optical fiber is technologically feasible and promises sensing performance higher than that obtainable with the conventional optical fibers. In addition, flat optical fiber can be embedded in composite materials reducing the drawbacks related to both orientation and excess resin.

Index Terms—Electromagnetic analysis, gratings, modeling, optical fiber devices, strain control.

I. INTRODUCTION

O PTICAL fiber sensor technology can be considered the state-of-the-art solution for monitoring the internal strain state of composite materials as carbon fiber reinforced polymer (CFRP), which is a material used in different areas, thanks to its advantages related to specific strength, high stiffness, and fatigue resistance [1], [2]. The employment of a non-destructive sensing approach is crucial to monitor the possibility of failures of the CFRP, such as cracks and delamination [3]–[8]. CFRP tends to be fragile in transverse directions and structural health

Francesco Anelli, Andrea Annunziato, Alessia Erario, Caterina Ciminelli, and Francesco Prudenzano are with the Department of Electrical and Information Engineering, Politecnico di Bari, 70125 Bari, Italy (e-mail: f.anelli3@ studenti.poliba.it; andrea.annunziato@poliba.it; a.erario@studenti.poliba.it; caterina.ciminelli@poliba.it; francesco.prudenzano@poliba.it).

Christopher Holmes is with the Optoelectronics Research Centre, University of Southampton, SO17 1BJ Southampton, U.K. (e-mail: christopher. holmes@southampton.ac.uk).

monitoring (SHM) can be successfully implemented using fiber Bragg gratings (FBGs) [9]. FBGs offer advantages in terms of dimension, weight, immunity to electromagnetic interference, multiplexing, low-cost, high spatial resolution, feasibility in harsh environment [10], [11]. Embedded FBG sensors can detect both static and dynamic strain fields [12]–[14]. The use of embedded optical fiber sensor for the detection of static strain in composite materials can be considered mature for uniaxial load [15]–[19]. With reference to multiaxial strain monitoring, high birefringent FBGs (i.e., microstructured, panda, bow-tie etc.) have been proposed, exploiting the differences in fast and slow axis sensitivities [20], [21]. The major drawback of high birefringent FBGs is related to the need of their precise orientation with respect to the composite material structure, since an a priori knowledge and control of fiber rotation is not always practical to obtain. Errors in orientation assessment lead to a wrong estimation of the strain field [22]. Moreover, the conventional cylindrical geometry, typical for the most of the high birefringent FBGs, causes, during the embedding process, the formation of a region around the optical fiber filled with epoxy resin which degrades the mechanical characteristics of the composite [23], [24].

Flat optical fiber shape is appropriate for the embedding process, mitigating both the problems related to resin-rich regions and to orientation. Flat optical fiber is essentially composed of a slab waveguide and a surrounding cladding [25]. In general, it can support multimode propagation in two lateral elliptical core regions, named "eyelets", and single mode propagation in the central core region due to the presence of a thin and flat core layer [26]. Single mode waveguides can be written, by inducing a further refractive index change, both in the eyelets and in the central core layer through direct UV writing (DUW) or femtosecond laser inscription [25], [27]. Many passive devices have been proposed in flat optical fibers such as gratings, resonators, splitters, interferometers and microfluidic channel [25], [28].

Flat optical fiber sensors can be used for the detection of damages, caused by impact, delamination or debonding, through the comparison of the spectrum before and after their manifestations and the use of detective algorithms for advanced pattern recognition [29]–[32].

In this paper, an innovative microstructured flat optical fiber (MFOF) is designed for multiparameter monitoring. To the best of our knowledge, for the first time, a feasible microstructured flat optical fiber is proposed to perform triaxial strain monitoring with high accuracy. The strain transfer from host material to the

sensor is accurately considered in the simulations; this aspect is crucial due to the differences in mechanical properties (e.g., density, Young's modulus, Poisson's ratio) between the optical fiber and composite material [33]. An FBG in both eyelets is designed and different transversal strain sensitivities are obtained due to the presence of a pattern of air holes running along the longitudinal direction of the optical fiber, in correspondence of only one of the two eyelets. The change of the reflection spectrum, i.e., the Bragg wavelength shift of each grating due to the applied stress, allows monitoring the internal strain state of CFRP.

The paper is organized as follows. In Section I, the introduction; in Section II, the operation principle, the MFOF description, the simulation approach and the validation of the model; in Section III, the geometrical and physical parameters of CFRP and designed MFOF; in Section IV, the numerical results are outlined and critically discussed with their implications for future works; in Section V, the conclusion is reported.

II. OPERATION PRINCIPLE AND MFOF DESCRIPTION

A flat optical fiber has a shape similar to that of a planar waveguide. It consists of a central core layer with two lateral larger multimode regions, typically named eyelets. The outstanding potential of flat optical fiber, mentioned in Section I, can be emphasized as a multiparameter sensor by performing a different design of the two eyelets to alter the strain distribution among them. The distribution and the number of the air holes of the microstructure can affect the sensor response. They can be used to convey stress in specific regions of the optical fiber [1], [34], [35]. Air holes number, pattern and position variation can lead to different strain field transferred to the microstructured eyelet resulting in change in sensitivity.

The sketch of the proposed flat optical fiber sensor is illustrated in Fig. 1(a). The two eyelets hosting the DUW waveguides, the central core layer and microstructure with air holes along the propagation direction are shown. For reading easiness, only the first air hole is shown in perspective view. Fig. 1(b) illustrates a sketch, not in scale, of the uncoated MFOF sensor, embedded on the sixth layer of a CFRP lamina which is made up of eight unidirectional layers. The sensor can be embedded in a different layer being the composite unidirectional.

The fabrication of the proposed flat optical fiber can be achieved through the use of modified chemical vapor deposition (MCVD). In previous fabrication approaches, the cylindrical preform, during the drawing process, has collapsed by creating the planar shape without microstructure [25]. In order to obtain the microstructure, collapse of the preform should be conducted prior to the drawing stage. Then, an ultrasonic mill can be employed to form the holes directly in the preform. As an alternative, holes can be obtained through milling an area into the preform and stacking appropriate silica canes. To avoid collapse or tapering of the microstructured holes, a positive gas pressure within air holes can be applied during the fiber draw process. Starting from few mbar, the pressure can be adjusted to get the required hole dimensions depending on original size of holes and outer preform dimension.
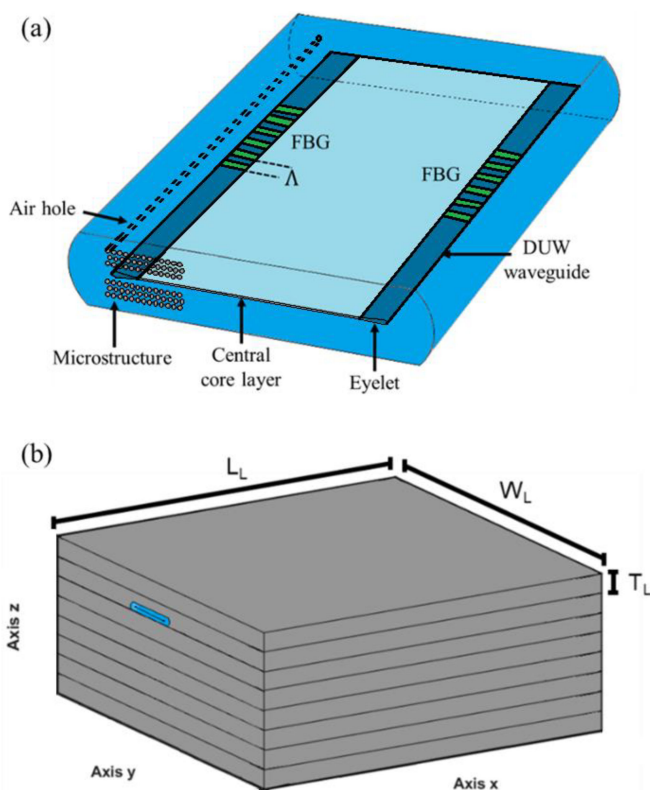

Fig. 1. Sketch of the MFOF with air holes surrounding one eyelet along the x axis (a). Schematic of the simulated CFRP lamina (grey) with MFOF sensor (blue) embedded. The lamina is unidirectional, and it is made of eight layers. Each layer has a thickness T_L, length L_L and a width W_L (b).

In a CFRP lamina, the effects of residual stresses caused by the curing process of the composite material can be divided in two main kinds: micro-level (difference in material properties leading to debonding or cracks) and macro-level (ply anisotropy, shape change due to temperature gradients) effects. They directly affect the mechanical deterioration of the composite with time [23], [36]–[39]. The anisotropic stress related to manufacturing process can alter the spectrum, which is split into two separated Bragg peaks, two for each grating, as if it was a high birefringent fiber in the case of cross-ply configuration [22]. However, in the design, these effects have been neglected since they are not significant with reference to the Bragg wavelength shift and, as a consequence, with reference to the sensitivity [40]. In addition, in composite lamina with unidirectional layer configuration, as that considered in this paper, the Bragg wavelength split due to the residual stress does not occur.

A. Design Approach

The design approach is summarized as follows: i) development of a 3D-FEM (Finite Element Method, via COMSOL Multiphysics) model of the CFRP lamina with the embedded optical fiber; ii) 2D-FEM mode analysis of the MFOF; iii) transfer matrix method (TMM) to calculate the influence of the strains on reflective spectrum of the gratings.

The 3D-FEM model allows an accurate calculation of the strain transfer from CFRP lamina to the embedded sensor for
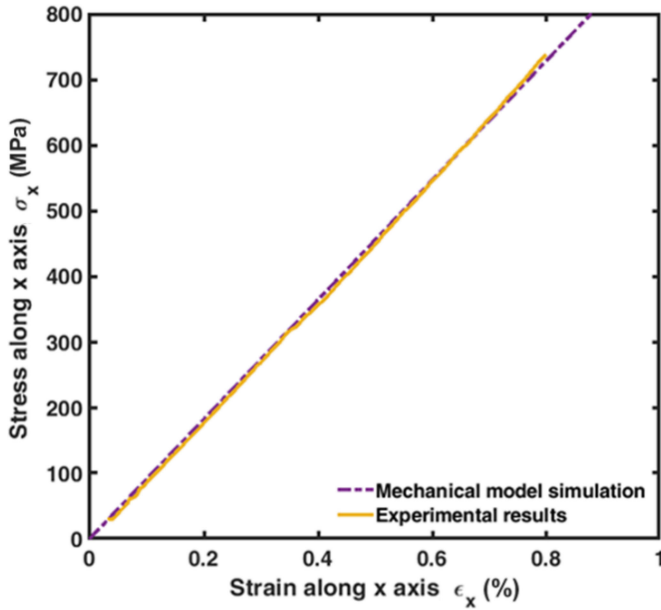
Fig. 2. Tensile stress σ_x versus strain ϵ_x along x axis: simulation via mechanical model (purple dash dotted curve), experimental results (yellow curve) [40].

Fig. 3. Simulated reflection spectra in absence of external loading ($\epsilon_x = 0\%$, dotted blue curve) and in presence of transverse cracks with crack density $\rho = 7\ cm^{-1}$ ($\epsilon_x = 0.42\%$, orange curve) of uniform silica FBG characterised by core diameter $d_{co} = 10\ \mu m$, cladding diameter $d_{cl} = 125\ \mu m$ and grating period $\Lambda = 530\ nm$.

stresses σ applied along x, y and z axis, see Fig. 1(b). The CFRP is modelled considering the micromechanical analysis of the unit cell, leading to the computation of the elasticity matrix $[E]_m$ [2]. The evaluated strains are employed to calculate the refractive index variation Δn of the optical guiding structure [2]. The effective refractive index of fundamental modes n_{eff} guided in the two eyelets can be computed through 2D-FEM mode analysis and used as input data for calculating the Bragg wavelength λ_B shift via TMM [41].

B. Model Validation

The model for simulating an embedded optical fiber sensor in CFRP laminate, has been validated. In particular, both the mechanical analysis of the composite material lamina and the electromagnetic modal investigation of the MFOF have been validated with literature results [40] for a CFRP lamina Toray T800H/3631 (Toray Industries, Inc) composed of eight layers in cross-ply configuration $[0_2/90_4/0_2]$.

Its physical properties are reported in [42]–[45]. A layer of composite lamina is characterized by a thickness $T_L = 0.15\ mm$, a length $L_L = 120\ mm$ and a width $W_L = 20\ mm$.

A micromechanical analysis on a single unit cell, made of carbon fiber and resin (carbon fiber-resin volume fraction $v_f = 0.6$), has been performed to evaluate the elasticity matrix $[E]_m$ of a layer as in [2].

In [40], the stress σ_x as a function of the strain ϵ_x is measured by means of strain gage. In the simulation performed to validate our model, the presence of the embedded fiber in the CFRP has been realistically considered. Fig. 2 illustrates the comparison between the simulated tensile stress σ_x versus the strain ϵ_x (purple dash dotted curve) with the measurement (yellow curve) reported in [40]: an excellent agreement is obtained.
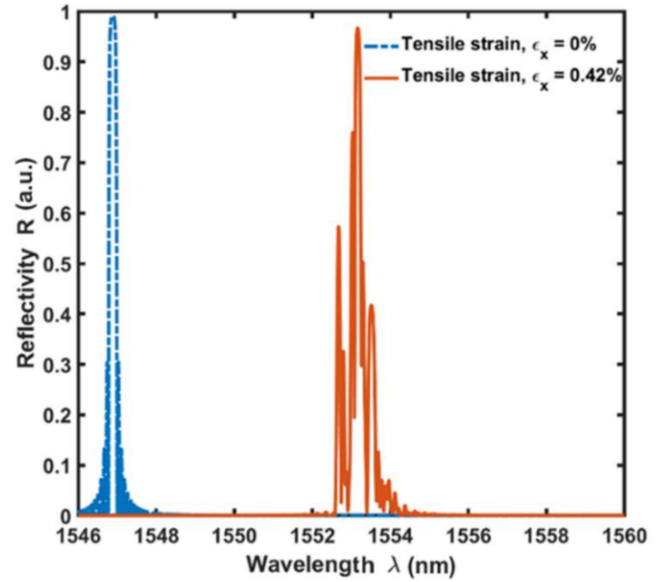
TABLE I
GEOMETRICAL PARAMETERS OF THE CFRP LAMINA

Parameter	Symbol	Value	Unit
Layer thickness	T_L	0.3	mm
Layer length	L_L	150	μm
Layer width	W_L	40	μm

Fig. 3 illustrates the simulated reflection spectra, in absence of external loading ($\epsilon_x = 0\%$, dotted blue curve) and in presence of transverse cracks with crack density $\rho = 7\ cm^{-1}$ ($\epsilon_x = 0.42\%$, orange curve), of uniform silica FBG with core diameter $d_{co} = 10\ \mu m$, cladding diameter $d_{cl} = 125\ \mu m$ and grating period $\Lambda = 530\ nm$.

The optical fiber lays on the sixth layer at the interface with the seventh. The obtained results are in excellent agreement with [40].

Therefore, the overall model and simulation approach has been validated in the case of an embedded uncoated FBG in presence of uniaxial non uniform strain as occurs in case of transverse cracks [40].

III. DESIGN OF THE EMBEDDED MFOF

The mechanical and electromagnetic investigation, performed for the embedded sensor design, realistically takes into account the geometry and the physical properties of both the optical fiber and the CFRP. In particular, the parameters regarding the carbon fiber and epoxy resin (carbon fiber-resin volume fraction is $v_f = 0.6$) are reported in Tables I and II [46].

The design of the proposed MFOF sensor for structural health monitoring applications aims to an efficient triaxial strain

TABLE II
PHYSICAL PARAMETERS OF THE CFRP LAMINA

Parameter	Symbol	Value carbon fiber	Value epoxy	Unit
Young's modulus	E	230 (x) 15 (y)	4	GPa
Shear modulus	G	24 (xy) 5.03 (yz)	–	GPa
Poisson's ratio	v	0.2 (xy) 0.07 (yz)	0.35	–
Density	ρ	1800	1100	kg/m^3

TABLE III
PHYSICAL PROPERTIES OF THE MFOF [46]

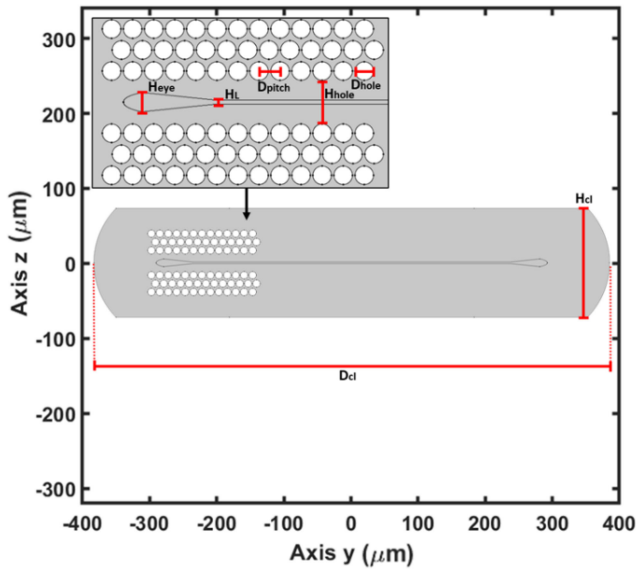| Parameter	Symbol	Value	Unit
Young's modulus	E	78.3	GPa
Poisson's ratio	v	0.186	–
Pockel's coefficient	$\rho 11$	0.121	–
Pockel's coefficient	$\rho 12$	0.27	–

Fig. 4.   Cross-section of the MFOF.

discrimination. It is closely related to the choice of a proper arrangement of the air holes along the optical fiber length. The sensor response to specific external perturbations can be optimized by varying the diameter, the pitch and the position of the air holes in the MFOF cross-section. It is worth noting that the range of these variations is limited by mechanical robustness, which decreases by increasing the air filling fraction.

Regarding the MFOF, the physical properties are reported in Table III. The cross-section of MFOF of Fig. 1(a) is reported in Fig. 4. The geometrical parameters and the physical properties of the MFOF such as the height of elliptical eyelets H_{eye}, the height of the central layer H_L, the height of the cladding H_{cl}, the length of the cladding D_{cl} are reported in Table IV [46]. These

TABLE IV
GEOMETRICAL PARAMETERS OF THE MFOF

Parameter	Symbol	Value	Unit
Height of elliptical eyelets	H_{eye}	13.71	μm
Height of the central layer	H_L	2.46	μm
Height of the cladding	H_{cl}	162.33	μm
Length of the cladding	D_{cl}	764.46	μm
Distance between the air holes	D_{pitch}	12.5	μm
Diameter of the air holes	D_{hole}	11	μm
Vertical distance between holes	H_{hole}	26	μm

geometrical parameters are realistic since they are pertaining to a fabricated flat optical fiber without microstructure [46].

DUW can be employed along the length of the flat optical fiber in correspondence of the eyelets, to avoid light propagation in the central core layer, and to guide the light only in the eyelets. The presence of air holes reduces the total flux of UV light at the fiber core. However, a periodic interference can still be obtained with longer exposure time despite the presence of scattering at the hole-silica interface [47], [48]. In particular, the cladding of the flat optical fiber is made of pure silica while the eyelet and the central core layer are doped with germanium and/or boron [26]. The local change of the refractive index in the eyelets with respect to the central core region is $\Delta n_{DUW} = 5 \times 10^{-3}$ [26]. The refractive index values are $n_{eye} = 1.4595$ for the eylets, $n_{cc} = 1.4590$ for the central core regions and $n_{cl} = 1.4439$ for the cladding at the wavelength $\lambda = 1560\ nm$.

For a flat optical fiber, without microstructure and without any stress external perturbations, having the aforesaid optical and geometrical parameters the simulated effective refractive index of the fundamental mode guided in the eyelet is $n_{eff} = 1.4579$ in perfect agreement with measurement [46].

Moreover, typical propagation loss of flat fiber is of the order $0.24\ dB/cm$ [49], ensuring, for the typical lengths required in structural health monitoring, low signal attenuation.

The design strategy has been focused on the microstructure refinement in order to reach the desired sensor response. It has required the choice of suitable dimensions for the distance between the air holes D_{pitch}, the diameter of the air holes D_{hole} and the vertical distance H_{hole} between the last row and the first row of the upper- and lower-holes distribution. In particular, the optimized microstructure has been obtained through several simulations via a trial-and-error approach, by performing both mechanical and electromagnetic investigations, according to the previously described design approach. The design criterion of the microstructure has been the sensitivity maximization of one eyelet to applied load. The main result is that a pattern of air holes, distributed only on an eyelet, with $D_{pitch} = 12.5\ \mu m$, $D_{hole} = 11\ \mu m$ and $H_{hole} = 26\ \mu m$ introduce an optimized strain distribution, very different with respect to that occurring in the eyelet without microstructure.
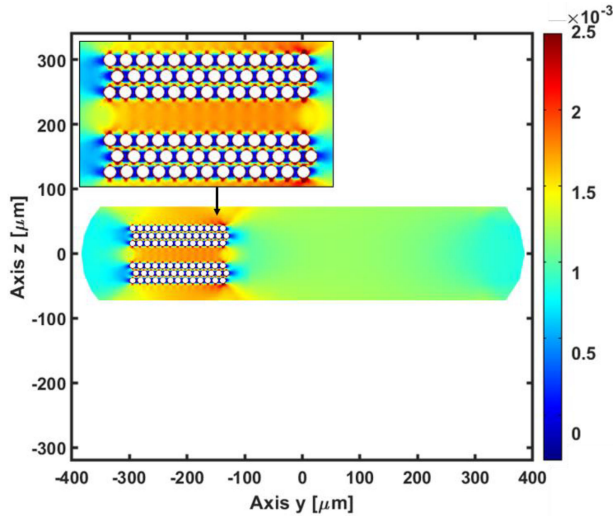
Fig. 5. Strain distribution ϵ_y in the cross-section of the MFOF embedded in the CFRP lamina, for a tensile stress $\sigma_y = 35\ MPa$ along the y axis.

This can clearly be explained by observing Fig. 5, that shows the strain distribution ϵ_y (y being the predominant component) in the cross-section of the MFOF embedded in the CFRP lamina, for a tensile stress $\sigma_y = 35\ MPa$ along the y axis. The presence of the air holes causes a more intense strain field in correspondence of the microstructured eyelet. Therefore, the designed pattern is suitable to increase the birefringence B of the microstructured eyelet when it is subjected to stress along the y axis σ_y. Birefringence B occurs because the two polarizations of the fundamental mode travel at different velocities, being characterized by distinct effective refractive indices: $n_{eff,fast}$ for the mode polarized along the fast axis, i.e., z axis, and $n_{eff,slow}$ for the mode polarized along the slow axis, i.e., y axis. The spacing $\Delta\lambda_B$ between the two Bragg peaks increases by increasing the birefringence B.

On the contrary, for stress applied along the z axis σ_z, the strain field distribution in the microstructured eyelet has lower module values and causes lower birefringence B with respect to the case of stress applied to eyelet without microstructure.

It is worth noting that, in the investigation, for each of mechanical stress component σ_x, σ_y, σ_z all the three principal induced strain components (ϵ_x, ϵ_y, ϵ_z) have been considered.

Fig. 6 shows the electric field norm distribution of the fundamental modes for the two eyelets at the wavelength $\lambda = 1560\ nm$; the simulated effective refractive index of the fundamental mode is $n_{eff} = 1.4579$ without external loading.

Uniform FBG with refractive index profile definition $\Delta n_{FBG} = 3 \times 10^{-4}$ is considered in both the eyelets. The nominal parameters of the gratings are listed in Table V (i.e., without/before applying external perturbations).

IV. RESULTS AND DISCUSSION

The refractive index change due to the applied stress has been calculated according to [2]. The propagation constants and the electromagnetic field distribution of the propagating modes have been simulated as described in Section II.
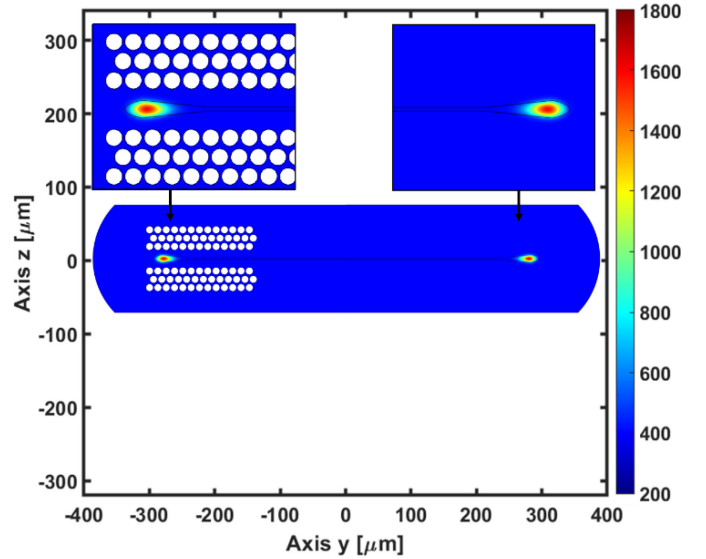

Fig. 6. Electric field norm distribution of the fundamental modes for the microstructured eyelet and the eyelet without microstructure, at the wavelength $\lambda = 1560\ nm$.

TABLE V
CHARACTERISTICS OF THE FIBRE BRAGG GRATINGS WITHOUT EXTERNAL
LOADING UNDER ISOTHERMAL CONDITION

| Parameter	Symbol	Value	Unit
Length of the grating	L	2000	μm
Grating period	Λ	0.5349	μm

The reflection spectra as a function of the stress have been evaluated for both the microstructured eyelet and the eyelet without microstructure, for both fast axis and slow axis. Four different sensitivities are calculated by ratio $\Delta\lambda_B/\Delta\sigma_i$ where the subscript $i = x$, y, z indicates the σ stress direction. They are: i) the fast axis propagation mode of the microstructured eyelet $K_{i,fm}$; ii) the slow axis propagation mode of the microstructured eyelet $K_{i,sm}$; iii) the fast axis propagation mode of the eyelet without microstructure $K_{i,f}$; iv) the slow axis propagation mode of the eyelet without microstructure $K_{i,s}$.

The longitudinal stress analysis, along the x axis, has been performed in the range from $\sigma_x = 0\ MPa$ to $\sigma_x = 90\ MPa$. The simulated Bragg wavelength λ_B versus the longitudinal stress σ_x determines four sensitivities that are very similar to each other. The influence of air holes is negligible in case of longitudinal stress σ_x. The sensitivities to stress along x axis σ_x are reported in Table VI.

Fig. 7 illustrates the Bragg wavelength λ_B as a function of the applied transverse stress along y axis σ_y, for both the microstructured eyelet and the eyelet without miscrostructure. In particular, the curves are pertaining to fast axis propagation mode of the microstructured eyelet (continuous blue), slow axis propagation mode of the microstructured eyelet (orange dashed), fast axis propagation mode of eyelet without microstructure (yellow dash dotted), and slow axis propagation mode of eyelet without microstructure (purple dotted). The response of the

TABLE VI
SENSITIVITY TO STRESS ALONG X AXIS σ_x

Parameter	Symbol	Value	Unit
Fast axis eyelet without microstructure	$K_{x,f}$	8.88	pm/MPa
Fast axis microstructured eyelet	$K_{x,fm}$	8.86	pm/MPa
Slow axis eyelet without microstructure	$K_{x,s}$	8.85	pm/MPa
Slow axis microstructured eyelet	$K_{x,sm}$	8.91	pm/MPa
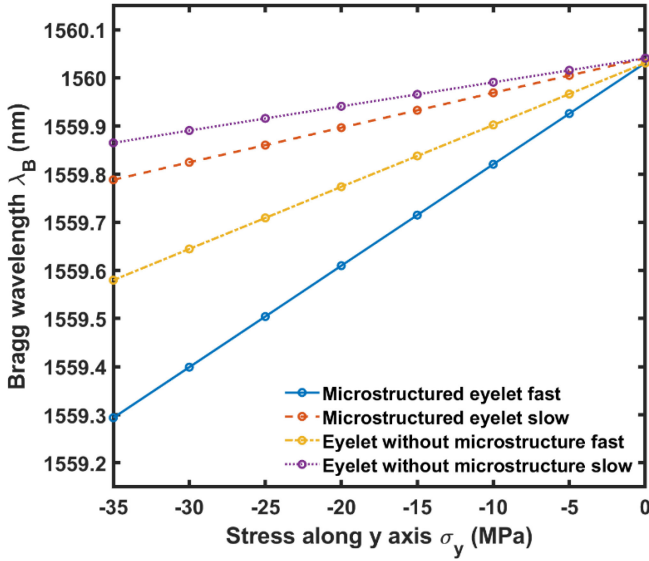
Fig. 7. Simulated Bragg wavelength λ_B versus the transverse stress σ_y: fast axis microstructured eyelet (continuous blue); slow axis microstructured eyelet (orange dashed); fast axis eyelet without microstructure (yellow dash dotted); slow axis eyelet without microstructure (purple dotted). Grating characteristics: $\Lambda = 0.5349\ \mu m$, $\Delta n_{FBG} = 3 \times 10^{-4}$, L = 2000 μm.

slow and fast axis for the microstructured eyelet is different with respect to that of the eyelet without microstructure. The presence of air holes alters the internal stress distribution in the MFOF cross-section. The internal stress, in a material with a hole, concentrates in the surface perpendicular to the direction of the applied load and passing through the center of the hole. By applying a stress along the y axis σ_y, the internal stress concentrates along the z axis in the microstructured eyelet region, as shown in Fig. 5. This causes a strong refractive index variation affecting the propagation mode characteristics and the Bragg wavelength λ_B.

Fig. 8 illustrates the Bragg wavelength λ_B as a function of the applied stress along z axis σ_z for the fast axis propagation mode of the microstructured eyelet (continuous blue), slow axis propagation mode of the microstructured eyelet (orange dashed), fast axis propagation mode of eyelet without microstructure (yellow dash dotted), and slow axis propagation mode of eyelet without microstructure (purple dotted). In this case, the sensitivity of the fast and slow axis of the eyelet without microstructure is larger than that of the microstructured eyelet. Since the air holes concentrates the internal stress distribution in the surface
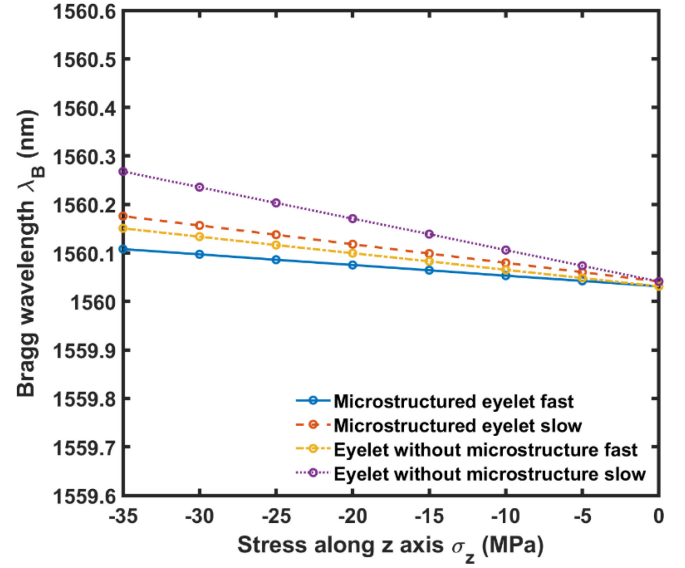

Fig. 8. Simulated Bragg wavelength λ_B versus the transverse stress σ_z: fast axis microstructured eyelet (continuous blue); slow axis microstructured eyelet (orange dashed); fast axis eyelet without microstructure (yellow dash dotted); slow axis eyelet without microstructure (purple dotted). Grating characteristics: $\Lambda = 0.5349\ \mu m$, $\Delta n_{FBG} = 3 \times 10^{-4}$, L = 2000 μm.

TABLE VII
SENSITIVITY TO STRESS ALONG Y AXIS σ_y

Parameter	Symbol	Value	Unit
Fast axis eyelet without microstructure	$K_{y,f}$	12.89	pm/MPa
Fast axis microstructured eyelet	$K_{y,fm}$	21.06	pm/MPa
Slow axis eyelet without microstructure	$K_{y,s}$	5.02	pm/MPa
Slow axis microstructured eyelet	$K_{y,sm}$	7.22	pm/MPa

TABLE VIII
SENSITIVITY TO STRESS ALONG Z AXIS σ_z

Parameter	Symbol	Value	Unit
Fast axis eyelet without microstructure	$K_{z,f}$	−3.42	pm/MPa
Fast axis microstructured eyelet	$K_{z,fm}$	−2.19	pm/MPa
Slow axis eyelet without microstructure	$K_{z,s}$	−6.48	pm/MPa
Slow axis microstructured eyelet	$K_{z,sm}$	−3.85	pm/MPa

perpendicular to the direction of the applied load σ_z, the stress is conveyed outside the microstructured eyelet, so that the air holes act as decreasing stress buffer. The sensitivities related to transverse stresses (i.e., σ_y and σ_z), for each polarization of the designed MFOF, are reported in Tables VII-VIII.

By simulation, the designed sensor exhibits a good feasibility with respect to typical fabrication tolerances. The strong difference of the sensitivity along the transversal directions enables an efficient triaxial stress detection. The combination of double grating and birefringence B induced by applied transverse

stresses creates four peaks/dips in the reflection/transmission spectrum. In theory, a fourth physical parameter could be monitored. The proposed device is sensitive to the stress along all directions. To perform triaxial stress detection, the linear model proposed in [50], [51] can be exploited. In this way, the stresses in the host material can be effectively derived from measured wavelength shift $\Delta\lambda$ making use of stress transfer matrix and sensitivity matrix [50], [51].

For a comparison with the state of the art, the longitudinal strain sensitivities along x axis of the sensor proposed in this paper are consistent with literature high performance solutions [50], [52], being equal to $S_x = 1.24 \, pm/\mu\epsilon$ for both eyelets and slightly higher than those reported in [13].

Generally, triaxial strain sensing reported in literature require complex approaches such as: i) the presence of different sensors embedded in the composite material or different positioning of the sensors for longitudinal, in-plane and out-of-plane monitoring [9], [22]; ii) cascade of two FBGs in a single polarization-maintaining optical fiber, one of which is shielded by a capillary, to reduce transverse strains [52]; iii) use of two cascaded FBGs operating at different wavelengths [50]. In the aforesaid cases, i.e., for high birefringent fibers, the precise control of fiber rotation/mode polarization orientation during embedding process decreases the effective feasibility.

We underline that the potential of the microstructured flat optical fiber proposed in this paper is related to the possibility of using only one optical fiber sensor without a precise control of its orientation. The flat optical fiber shape mitigates the problem related to resin-rich regions of circular optical fibers. The inscription of a cascade of FBGs enables the possibility to map strains with high spatial resolution, exploiting wavelength division multiplexing. Therefore, the designed microstructured flat fiber paves the way for a feasible multiaxial structural health monitoring.

V. Conclusion

A novel microstructured flat optical fiber for multiparameter sensing in CFRP lamina has been designed. The air hole microstructured pattern in correspondence of one eyelet alter the strain transfer between composite lamina and the guiding region. The strain-transfer and the electromagnetic modal analysis have led to the calculation of different transverse sensitivities for the two FBGs written in the eylets. The relevant advantage introduced by the use of the designed microstructure is evident with regard to the slow and fast y axis sensitivities $K_{y,f} = 12.89 \, pm/MPa$, $K_{y,fm} = 21.06 \, pm/MPa$, $K_{y,s} = 5.02 \, pm/MPa$, $K_{y,sm} = 7.22 \, pm/MPa$, yielding to high sensitivity triaxial strain detection. Moreover, flat optical fiber shape agevolates the embedding process, reducing the drawbacks due to resin-rich regions of circular optical fibers and orientation of high birefringent optical fibers.

Acknowledgment

References

[1] C. Sonnenfeld et al., "Microstructured optical fiber sensors embedded in a laminate composite for smart material applications," *Sensors*, vol. 11, no. 3, pp. 2566–2579, 2011, doi: 10.3390/s110302566.

[2] A. Annunziato, F. Anelli, J. Gates, C. Holmes, and F. Prudenzano, "Design of polarization-maintaining FBGs using polyimide films to improve strain-temperature sensing in CFRP laminates," *IEEE Photon. J.*, vol. 13, no. 2, Apr. 2021, Art. no. 7100315, doi: 10.1109/JPHOT.2021.3063172.

[3] T. Vella et al., "Full-spectrum interrogation of fiber Bragg gratings at 100 kHz for detection of impact loading," *Meas. Sci. Technol.*, vol. 21, no. 9, 2010, Art. no. 094009, doi: 10.1088/0957-0233/21/9/094009.

[4] H.-P. Wang, Y.-Q. Ni, J.-G. Dai, and M.-D. Yuan, "Interfacial debonding detection of strengthened steel structures by using smart CFRP-FBG composites," *Smart Mater. Struct.*, vol. 28, no. 11, 2019, Art. no. 115001, doi: 10.1088/1361-665X/ab3add.

[5] S. Takeda, Y. Okabe, and N. Takeda, "Monitoring of delamination growth in CFRP laminates using chirped FBG sensors," *J. Intell. Mater. Syst. Struct.*, vol. 19, no. 4, pp. 437–444, 2008, doi: 10.1177/1045389X06074085.

[6] S. Takeda, Y. Okabe, and N. Takeda, "Delamination detection in CFRP laminates with embedded small-diameter fiber Bragg grating sensors," *Comp. Part A: Appl. Sci. Manuf.*, vol. 33, no. 7, pp. 971–980, 2002, doi: 10.1016/S1359-835X(02)00036-2.

[7] A. Rajabzadeh, R. Heusdens, R. C. Hendriks, and R. M. Groves, "Characterisation of transverse matrix cracks in composite materials using fibre Bragg grating sensors," *J. Lightw. Technol.*, vol. 37, no. 18, pp. 4720–4727, Sep. 2019, doi: 10.1109/JLT.2019.2919339.

[8] P. Zhu, P. Liu, Z. Wang, C. Peng, N. Zhang, and M. A. Soto, "Evaluating and minimizing induced microbending losses in optical fiber sensors embedded into glass-fiber composites," *J. Lightw. Technol.*, vol. 39, no. 22, pp. 7315–7325, Nov. 2021, doi: 10.1109/JLT.2021.3112484.

[9] C. Holmes, M. Godfrey, D. J. Bull, and J. Dulieu-Barton, "Real-time through- thickness and in-plane strain measurement in carbon fibre reinforced polymer composites using planar optical Bragg gratings," *Opt. Lasers Eng.*, vol. 133, 2020, Art. no. 106111, doi: 10.1016/j.optlaseng.2020.106111.

[10] G. Pereira, C. Frias, H. Faria, O. Frazão, and A. Marques, "On the improvement of strain measurements with FBG sensors embedded in unidirectional composites," *Polym. Testing*, vol. 32, no. 1, pp. 99–105, 2013, doi: 10.1016/j.polymertesting.2012.09.010.

[11] J. Chen, B. Liu, and H. Zhang, "Review of fiber Bragg grating sensor technology," *Front. Optoelectron. China*, vol. 4, pp. 204–212, 2011, doi: 10.1007/s12200-011-0130-4.

[12] J. Frieden, J. Cugnoni, J. Botsis, and T. Gmür, "Low energy impact damage monitoring of composites using dynamic strain signals from FBG sensors—Part I: Impact detection and localization," *Comp. Struct.*, vol. 94, no. 2, pp. 438–445, 2012, doi: 10.1016/j.compstruct.2011.08.003.

[13] J. Frieden, J. Cugnoni, J. Botsis, and T. Gmür, "Low energy impact damage monitoring of composites using dynamic strain signals from FBG sensors—Part II: Damage identification," *Comp. Struct.*, vol. 94, no. 2, pp. 593–600, 2012, doi: 10.1016/j.compstruct.2011.08.025.

[14] G. Cazzulani, S. Cinquemani, L. Comolli, A. Gardella, and F. Resta, "Vibration control of smart structures using an array of fiber Bragg grating sensors," *Mechatron*, vol. 24, no. 4, pp. 345–353, 2014, doi: 10.1016/j.mechatronics. 2013.07.014.

[15] Z.-S. Guo, "Strain and temperature monitoring of asymmetric composite laminate using FBG hybrid sensors," *Struct. Health Monit.*, vol. 6, no. 3, pp. 191–197, 2007, doi: 10.1177/14759217070060030201.

[16] V. Antonucci, M. Esposito, M. Ricciardi, M. Giordano, and M. Zarrelli, "Strain monitoring of composite elements by fibre Bragg grating sensors during a quasi-static indentation," *Comp. Part B Eng.*, vol. 56, pp. 34–41, 2014, doi: 10.1016/j.compositesb.2013.07.020.

[17] M. Basu and S. Ghorai, "Strain sensing in fiber-reinforced polymer laminates using embedded fiber Bragg grating sensor," *Fiber Integr. Opt.*, vol. 33, no. 4, pp. 279–298, 2014, doi: 10.1080/01468030.2014.906686.

[18] A. Güemes, A. Fernández-López, P. F. Díaz-Maroto, A. Lozano, and J. Sierra- Perez, "Structural health monitoring in composite structures by fiber-optic sensors," *Sensors*, vol. 18, no. 4, 2018, doi: 10.3390/s18041094.

[19] G. Rajan, M. Ramakrishnan, Y. Semenova, E. Ambikairajah, G. Farrell, and G. D. Peng, "Experimental study and analysis of a polymer fiber Bragg grating embedded in a composite material," *J. Lightw. Technol.*, vol. 32, no. 9, pp. 1726–1733, May 2014, doi: 10.1109/JLT.2014.2311441.

[20] C. Jewart et al., "Sensitivity enhancement of fiber Bragg gratings to transverse stress by using microstructural fibers," *Opt. Lett.*, vol. 31, no. 15, pp. 2260–2262, 2006, doi: 10.1364/OL.31.002260.

[21] F. Bosia, P. Giaccari, J. Botsis, M. Facchini, H. G. Limberger, and R. P. Salathé, "Characterization of the response of fibre Bragg grating sensors subjected to a two-dimensional strain field," *Smart Mater. Struct.*, vol. 12, no. 6, pp. 925, 2003, doi: 10.1088/0964-1726/12/6/009.

[22] G. Luyckx, E. Voet, N. Lammens, W. De Waele, and J. Degrieck, "Residual strain-induced birefringent FBGs for multi-axial strain monitoring of CFRP composite laminates," *NDT E Int.*, vol. 54, pp. 142–150, 2013, doi: 10.1016/j.ndteint.2012.11.008.

[23] G. Luyckx, E. Voet, N. Lammens, and J. Degrieck, "Strain measurements of composite laminates with embedded fibre Bragg gratings: Criticism and opportunities for research," *Sensors*, vol. 11, no. 1, pp. 384–408, 2011, doi: 10.3390/s110100384.

[24] R. Di Sante, "Fibre optic sensors for structural health monitoring of aircraft composite structures: Recent advances and applications," *Sensors*, vol. 15, no. 8, pp. 18666–18713, 2015, doi: 10.3390/s150818666.

[25] K. Kalli et al., "Flat fibre and femtosecond laser technology as a novel photonic integration platform for optofluidic based biosensing devices and lab-on-chip applications: Current results and future perspectives," *Sens. Actuators B Chem.*, vol. 209, pp. 1030–1040, 2015, doi: 10.1016/j.snb.2014.12.003.

[26] G.-D. Peng, *Handbook of Optical Fibers*. Berlin, Germany: Springer, 2019.

[27] K. D. Dambul et al., "Fabrication and characterization of Ge-doped flat fibres," *J. Modern Opt.*, vol. 66, no. 11, pp. 1219–1225, 2019, doi: 10.1080/09500340.2019.1610518.

[28] F. R. M. Adikan et al., "Direct UV written optical waveguides in flexible glass flat fiber chips," *IEEE J. Sel. Topics Quantum Electron.*, vol. 18, no. 5, pp. 1534–1539, Sep.-Oct. 2011, doi: 10.1109/JSTQE.2011.2171921.

[29] T. H. Loutas, A. Panopoulou, D. Roulias, and V. Kostopoulos, "Intelligent health monitoring of aerospace composite structures based on dynamic strain measurements," *Expert Syst. Appl.*, vol. 39, no. 9, pp. 8412–8422, 2012, doi: 10.1016/j.eswa.2012.01.179.

[30] A. Propst et al., "Assessment of damage in composite laminates through dynamic, full-spectral interrogation of fiber Bragg grating sensors," *Smart Mater. Struct.*, vol. 19, no. 1, 2009, Art. no. 015016, doi: 10.1088/0964-1726/19/1/015016.

[31] A. Papantoniou, G. Rigas, and N. D. Alexopoulos, "Assessment of the strain monitoring reliability of fiber Bragg grating sensor (FBGs) in advanced composite structures," *Comp. Struct.*, vol. 93, no. 9, pp. 2163–2172, 2011, doi: 10.1016/j.compstruct.2011.03.001.

[32] S. Minakuchi, Y. Okabe, T. Mizutani, and N. Takeda, "Barely visible impact damage detection for composite sandwich structures by optical-fiber-based distributed strain measurement," *Smart Mater. Struct.*, vol. 18, no. 8, 2009, Art. no. 085018, doi: 10.1088/0964-1726/18/8/085018.

[33] E. Voet, G. Luyckx, W. De Waele, and J. Degrieck, "Multi-axial strain transfer from laminated CFRP composites to embedded Bragg sensor: II. Experimental validation," *Smart Mater. Struct.*, vol. 19, no. 10, 2010, Art. no. 105018, doi: 10.1088/0964-1726/19/10/105018.

[34] T. Martynkien et al., "Highly birefringent microstructured fibers with enhanced sensitivity to hydrostatic pressure," *Opt. Exp.*, vol. 18, no. 14, pp. 15113–15121, 2010, doi: 10.1364/OE.18.015113.

[35] T. Geernaert et al., "Transversal load sensing with fiber Bragg gratings in microstructured optical fibers," *IEEE Photon. Technol. Lett.*, vol. 21, no. 1, pp. 6–8, Jan. 2008, doi: 10.1109/LPT.2008.2007915.

[36] H.-S. Kim, S.-H. Yoo, and S.-H. Chang, "In situ monitoring of the strain evolution and curing reaction of composite laminates to reduce the thermal residual stress using fbg sensor and dielectrometry," *Comp. Part B Eng.*, vol. 44, no. 1, pp. 446–452, 2013, doi: 10.1016/j.compositesb.2012.04.021.

[37] K.-P. Ma, C.-W. Wu, Y.-T. Tsai, Y.-C. Hsu, and C.-C. Chiang, "Internal residual strain measurements in carbon fiber-reinforced polymer laminates curing process using embedded tilted fiber Bragg grating sensor," *Polymers*, vol. 12, no. 7, 2020, doi: 10.3390/polym12071479.

[38] J. Oelhafen, T. Mayr, F. Dorner, K. Moutzouris, J. Roths, and K. Drechsler, "Fiber optic measurement system for Fresnel reflection sensing: Calibration, uncertainty, and exemplary application in temperature-modulated isothermal polymer curing," *J. Lightw. Technol.*, vol. 36, no. 4, pp. 939–945, Feb. 2018, doi: 10.1109/JLT.2017.2757525.

[39] N. Zobeiry and A. Poursartip, "The origins of residual stress and its evaluation in composite materials," in *Structural Integrity and Durability of Advanced Composites*. Sawston, U.K.: Woodhead Publishing, 2015, pp. 43–72.

[40] Y. Okabe, S. Yashiro, T. Kosaka, and N. Takeda, "Detection of transverse cracks in CFRP composites using embedded fiber Bragg grating sensors," *Smart Mater. Struct.*, vol. 9, no. 6, pp. 832, 2000, doi: 10.1088/0964-1726/9/6/313.

[41] T. Erdogan, "Fiber grating spectra," *J. Lightw. Technol.*, vol. 15, no. 8, pp. 1277–1294, 1997, doi: 10.1109/50.618322.

[42] R. Potluri, "Mechanical properties evaluation of T800 carbon fiber reinforced hybrid composite embedded with silicon carbide microparticles: A micromechanical approach," *Multidiscipline Model. Mater. Struct.*, vol. 14, no. 3, pp. 589–608, 2018, doi: 10.1108/MMMS-09-2017-0106.

[43] M. Rodríguez, J. M. Molina-Aldareguía, C. González, and J. LLorca, "A methodology to measure the interface shear strength by means of the fiber push-in test," *Comp. Sci. Technol.*, vol. 72, no. 15, pp. 1924–1932, 2012, doi: 10.1016/j.compscitech.2012.08.011.

[44] L. St-Pierre, N. J. Martorell, and S. T. Pinho, "Stress redistribution around clusters of broken fibres in a composite," *Comp. Struct.*, vol. 168, pp. 226–233, 2017, doi: 10.1016/j.compstruct.2017.01.084.

[45] D. Chung, *Carbon Fiber Composites*. Amsterdam, The Netherlands: Elsevier, 2012.

[46] A. Annunziato, F. Anelli, M. Godfrey, J. M. Barton, C. Holmes, and F. Prudenzano, "Design of flat optical fiber sensor for triaxial strain monitoring in composite laminates," in *Proc. IEEE AEIT Int. Annu. Conf.*, 2021, pp. 1–6, doi: 10.23919/AEIT53387.2021.9626867.

[47] H. R. Sørensen, J. Laegsgaard, J. Canning, K. Hansen, and P. Varming, "Liquid filling of photonic crystal fibres for grating writing," *Opt. Commun.*, vol. 270, no. 2, pp. 207–210, 2007, doi: 10.1016/j.optcom.2006.09.009.

[48] T. Geernaert et al., "Bragg grating inscription in GeO$_2$-doped microstructured optical fibers," *IEEE J. Lightw. Technol.*, vol. 28, no. 10, pp. 1459–1467, May 2010, doi: 10.1109/JLT.2010.2043414.

[49] S. Ambran et al., "A loss comparison of flat-fibre and silica-on-silicon direct UV written waveguides using a novel Bragg grating measurement technique," in *Proc. Photon 10th Conf.*, Southampton, U.K. Aug. 22–25, 2010. [Online]. Available: https://eprints.soton.ac.uk/340787/1/4642.pdf

[50] T. Mawatari and D. Nelson, "A multi-parameter Bragg grating fiber optic sensor and triaxial strain measurement," *Smart Mater. Struct.*, vol. 17, no. 3, 2008, Art. no. 035033, doi: 10.1088/0964-1726/17/3/035033.

[51] C. Sonnenfeld et al., "Microstructured optical fiber Bragg grating as an internal three-dimensional strain sensor for composite laminates," *Smart Mater. Struct.*, vol. 24, no. 5, 2015, Art. no. 055003, doi: 10.1088/0964-1726/24/5/055003.

[52] G. Luyckx et al., "Three-dimensional strain and temperature monitoring of composite laminates," *Insight-Non-Destructive Testing Condition Monit.*, vol. 49, no. 1, pp. 10–16, 2007, doi: 10.1784/insi.2007.49.1.10.

Francesco Anelli received the M.Sc. degree in electronic engineering (cum laude), in 2021, from Politecnico di Bari, Bari, Italy, where he is a Ph.D. student in electrical and information engineering. His research interests include the modeling and the characterization of optical fiber grating sensors and optical devices for multispectral gas monitoring.

Andrea Annunziato received the M.Sc. degree in electronic engineering (cum laude) from Politecnico di Bari, Bari, Italy, in 2020. During his thesis he was at the University of Southampton, Southampton, U.K., where he conducted research on high birefringent optical fibers and FBG sensors embedded in composites laminates for structural monitoring in aerospace applications. He is currently a Ph.D. student in engineering and aerospace sciences. His research interests include the modeling and the characterization of fiber lasers, optical fiber sensors and optical devices for aerospace applications.

Alessia Erario received the M.Sc. degree in electronic engineering (cum laude) from Politecnico di Bari, Bari, Italy, in 2020. During her thesis she was at the University of Southampton, Southampton U.K., where she conducted research on high birefringent optical fibers and FBG sensors embedded in composites laminates for structural monitoring in aerospace applications.

Christopher Holmes is a Royal Society Industry Fellow with GE Aviation and a Senior Enterprise Fellow at the Optoelectronics Research Centre, University of Southampton, Southampton, U.K. leading activity within the Aerolaser Lab. He is on the Board of Directors for the Gas Analysis and Sensing Group Ltd; Senior Member of Optica; Associate Editor for IET Science, Measurement and Technology and Chair of Optica Technical Group, Optical Fabrication and Testing.

Caterina Ciminelli received the Laurea degree in electronic engineering and the Ph.D. in electronic engineering, both from Politecnico di Bari, Bari, Italy, in 1996 and 2000, respectively. From 1999 to 2002, she did industrial research activity on optoelectronic devices and subsystems with the R&D Division of Pirelli Optical Systems, Milan, Italy, and Cisco Photonics Italy, Monza, Italy. In May 2002, she joined Politecnico di Bari as an Assistant Professor of Electronics and in 2012 she became an Associate Professor. Since August 2021, she has been a Full Professor of Electronics with Politecnico di Bari, where she has been the scientific responsible for the Optoelectronics Laboratory, since 2002. She was a visiting student with the Research Center of Alcatel, Marcoussis, France, in 1999, and a Visiting Researcher with Glasgow University, Glasgow, U.K., in 2004. She has authored or coauthored of more than 200 journal articles and conference papers. She is involved in several research projects, also as a Scientific Coordinator. Her research interests include integrated optoelectronics and photonics. She is a co-inventor of a patent. From January 2007 to December 2010, she was a Member of the Board of Directors of the Italian Society for Optics and Photonics. From 2012 to 2018, she was a Member of the Board of Directors of the Italian Electronic Society. She is currently a Member of the Italian Chapter of the IEEE Photonics Society. She is a Senior Member of the Optical Society of America and IEEE.

Francesco Prudenzano (Member, IEEE) received the Ph.D. degree in electronic engineering from Politecnico di Bari, Italy, in November 1996. Since 2018, he has been a Full Professor in Electromagnetic Fields with the Department of Electrical and Information Engineering, Politecnico di Bari, Italy. He is currently the Head of Microwave and Optical Engineering Group, Department of Electrical and Information Engineering, Politecnico di Bari. From 2016 to 2015 vice Chair and from 2017 to 2018 Chair of SIOF, the Italian Society of Optics and Photonics (Italian branch of EOS—European Optical Society). Member of Politecnico di Bari Board Directors. From 2016 to 2021 Chair of Teacher Council of the first level degree in Electronic and Communication Engineering; since 2021 Chair of the second level degree in Communication Engineering. He is involved in several national and international research and cooperation projects, also with the role of Scientific Coordinator. Project Leader and co-Leader within COST MP0702 and MP1401, actions in the field of photonics. Chair of national and international conferences. He has coauthored more than 450 publications, many of which got published in journals and international conferences, lectures, and invited papers.